AJNR

High-Resolution 7T MR Imaging of the Trochlear Nerve

T. Kumar, G.M. Virador, P. Brahmbhatt, A.A. Bhatt, E.H. Middlebrooks, A. Desai, A. Agarwal, P. Vibhute and V. Gupta

AJNR Am J Neuroradiol published online 19 January 2023
http://www.ajnr.org/content/early/2023/01/19/ajnr.A7774

Published January 19, 2023 as 10.3174/ajnr.A7774

High-Resolution 7T MR Imaging of the Trochlear Nerve

T. Kumar, G.M. Virador, P. Brahmbhatt, A.A. Bhatt, E.H. Middlebrooks, A. Desai, A. Agarwal, P. Vibhute, and V. Gupta

ABSTRACT

BACKGROUND AND PURPOSE: The trochlear nerve has traditionally been difficult to identify on MR imaging. The advent of 7T MR imaging promises to greatly benefit visualization of small structures due to gains in the signal-to-noise ratio allowing improved spatial resolution. We investigated the utility of a clinically feasible ultra-high-resolution 7T MR imaging protocol for identification of the trochlear nerve, as well as assessment of normal trochlear nerve anatomy.

MATERIALS AND METHODS: Coronal high-resolution 2D T2-weighted TSE images used in a 7T epilepsy protocol of 50 subjects at our institution were reviewed by 2 independent radiologists for visualization of the trochlear nerve at the nerve origin and cisternal, tentorial, and cavernous segments. The frequency of nerve visibility within these segments and their anatomy were documented, and disagreements were resolved by joint review.

RESULTS: Of the 100 nerves reviewed in 50 subjects, at least 2 segments of the trochlear nerve from the brainstem to the cavernous sinus were identified in 100% of cases. The origins from the brainstem and cisternal segment were visible in 65% and 93% of nerves, respectively. The trochlear nerve was identified at the trochlear groove in 100% of cases and in the posterior wall of the cavernous sinus in 74% of cases.

CONCLUSIONS: Coronal high-resolution 2D TSE at 7T reliably identified the trochlear nerve throughout its course and is a promising tool for imaging patients with suspected trochlear nerve pathology.

ABBREVIATIONS: CN = cranial nerve; SAR = specific absorption rate; SCA = superior cerebellar artery

The trochlear nerve, or cranial nerve IV (CN IV), provides motor innervation of the superior oblique muscle and is responsible for inferior abduction of the eye. As a purely motor nerve, trochlear nerve palsy presents as torsional diplopia with a characteristic compensatory head tilt away from the affected side.[1,2] Numerous disease processes including trauma, microvascular ischemia, or mass effect from a nearby tumor can affect the nerve, in addition to congenital trochlear nerve anomalies.[3] Iatrogenic trochlear nerve injury is also an important concern in skull base surgery. It is, therefore, important for the radiologist to be able to visualize the course of the trochlear nerve.

The trochlear nerve has the longest intracranial course of all cranial nerves (60 mm), while also having the smallest diameter of approximately 0.3–1 mm.[4,5] The course of the nerve has been divided into the brainstem, cisternal, tentorial, cavernous, and orbital segments.[6] The brainstem segment refers to the intra-axial course from the nucleus to the exit of the nerve into the quadrigeminal cistern. The longest segment, the cisternal segment, runs in the ambient cistern. The nerve then courses along the tentorium in its tentorial segment before piercing the dura within the trochlear cistern to enter the cavernous sinus. After coursing in the lateral wall of the cavernous sinus, the nerve enters the orbit through the superior orbital fissure, bifurcates, and innervates the superior oblique muscle.

The ability to identify the normal course of the trochlear nerve on imaging may serve as an aid to identify lesions or impingement by nearby structures. However, due to its small caliber and its course along several vascular structures, CN IV has been difficult to identify on imaging.[5] Delineating its intracranial course has remained challenging even with the state-of-the-art 3T MR imaging sequences, largely due to limits on achievable resolution. An intrinsically higher SNR on 7T offers the potential for ultra-high-resolution imaging and improved visualization of the trochlear nerve.[7] However, many substantial challenges of ultra-high-field MR imaging, such as B_0 and B_1+ inhomogeneity and an

Received November 8, 2022; accepted after revision December 31.

From the Department of Radiology, Mayo Clinic, Jacksonville, Florida.

Please address correspondence to Vivek Gupta, MD, 4500 San Pablo Rd S, Jacksonville, FL 32224; e-mail: gupta.vivek@mayo.edu

http://dx.doi.org/10.3174/ajnr.A7774

increased specific absorption rate (SAR), are barriers to reliable visualization of the trochlear nerve at 7T.[8] Careful sequence optimization is required to realize the full potential of ultra-high-field MR imaging. The purpose of this study was to investigate the utility of an optimized T2 TSE at 7T in identifying the trochlear nerve from its origin from the brainstem to the cavernous sinus and describe its anatomic relationships and normal variations.

MATERIALS AND METHODS

MR Imaging Technique

Based on the nerve diameter and orientation of its intracranial course, the optimal sequence considerations include coronal section orientation along the vertical axis of the midbrain (orthogonal to the nerve) with the shortest achievable section thickness to reduce volume averaging, in-plane resolution of ≥0.4 mm, high nerve-CSF contrast, coverage from posterior midbrain to midorbit, and acquisition time of ≤10 minutes for practical clinical utility. Coronal 2D T2-weighted TSE in clinical use for evaluation of the mesial temporal lobe in our recently implemented epilepsy protocol on a clinical 7T Magnetom Terra MR imaging scanner (Siemens) met all the above considerations.

Trochlear nerve segment visualization

	Total Nerve Visualization
Origin at brainstem	65/100 (65%)
Cisternal segment	93/100 (93%)
Tentorial segment	100/100 (100%)
Cavernous segment[a]	74/100 (74%)

[a] Only the posterior cavernous segment was visible.

Relevant sequence parameters included the following: section thickness = 1.2 mm, TR = 8630 ms, TE = 35 ms, flip angle = 138°, echo-train length = 10, FOV = 150 × 150 mm, in-plane resolution = 0.34 × 0.34 mm (reconstructed at an interpolated voxel size of 0.17 × 0.17 × 1.2 mm), and a total scan time of 8 minutes. This sequence was developed at our institution through extensive volunteer testing with multiple iterations of sequence parameter optimization of contrast and SNR for the desired resolution within a clinically acceptable scan time. Epilepsy is one of the most common clinical indications for 7T MR imaging at our institution, providing a large imaging data set. Furthermore, in this patient cohort, the brainstem and cisternal structures were expected to be normal.

Subjects and Data Acquisition

Scans of 60 consecutive subjects undergoing clinical 7T MR imaging for epilepsy were evaluated, of which 10 scans were excluded from the analysis owing to excessive motion. The age range of the subjects was 16–85 years (mean age, 40.7 years). None of the subjects had any reported history of diplopia or ocular movement disorder.

The coronal T2 TSE images from this data set were evaluated independently by 2 experienced neuroradiologists for identification of each trochlear nerve. Visualization of the nerve was recorded in a binary fashion for each segment: 1) origin from the midbrain, 2) cisternal segment, 3) tentorial segment, and 4) anterior portion of its cavernous segment. Satisfactory identification of the nerve was considered positive in each segment if the nerve was clearly visible in at least ≥2 consecutive sections. The course of the trochlear nerve was followed and recorded from its origin from the brainstem, through the ambient cistern, along the tentorium, and into the posterior cavernous sinus. Any disagreements in identification of the nerve between the 2 observers were resolved by joint review. The relationship of the nerve to the major arteries was also recorded, along with the anatomic features of the trochlear groove and the trochlear cistern. The diameter of the nerve in the ambient cistern and measurements of the trochlear groove were also documented.

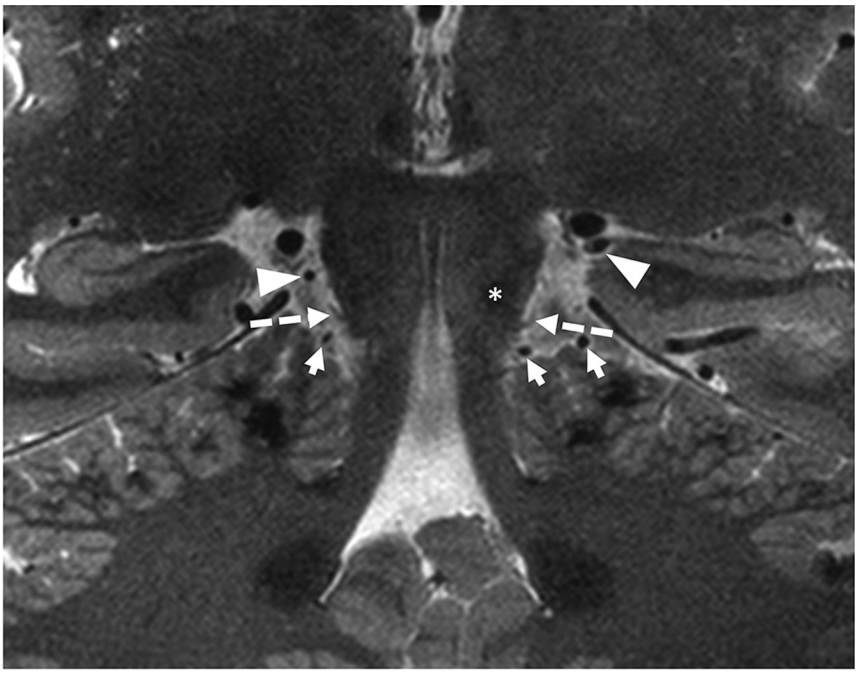

FIG 1. Coronal T2-weighted image showing the origins of trochlear nerve at the pontomesencephalic junction along the posterior aspect of the brainstem (*dashed arrows*), the left inferior colliculus (*asterisk*), rostral branches of the SCA (*arrowheads*), and caudal branches of the SCA (*short arrows*).

RESULTS

The incidence of positive identification of the different nerve segments is recorded in the Table. Of the 100 nerves reviewed in 50 subjects, at least some part of each trochlear nerve was identified in 100% of cases. The overall interrater agreement in identification of the nerve segments was 93% ($\kappa = 0.76$).

Of the total 100 nerves studied, the origin from the brainstem immediately below the inferior colliculus was confidently identified in 65% and the nerve

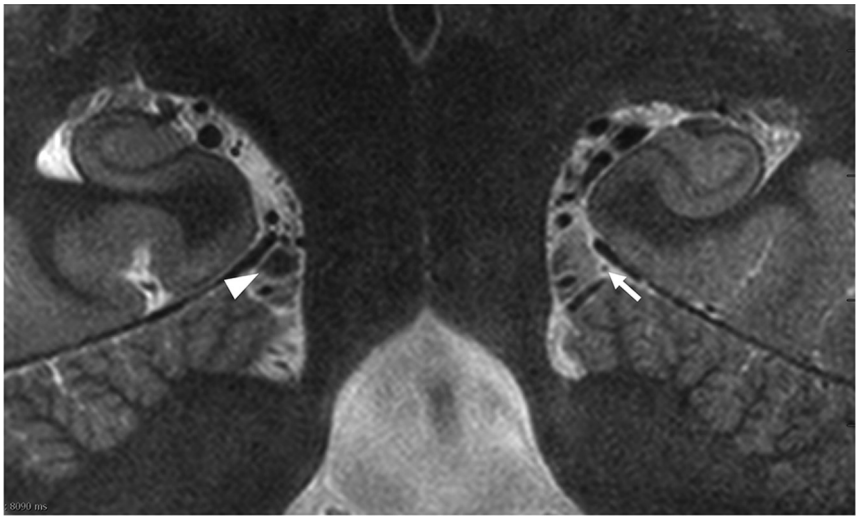

FIG 2. Coronal T2-weighted image showing the left trochlear nerve within the ambient cistern coursing toward the tentorium cerebelli (*arrow*). Note CSF flow signal obscuring the right trochlear nerve (*arrowhead*).

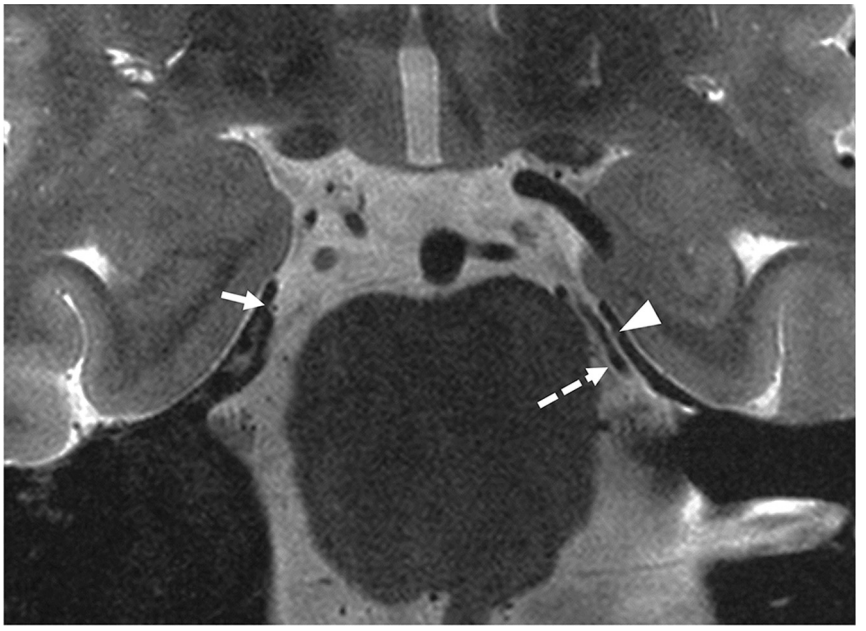

FIG 3. Coronal T2-weighted image showing the left trochlear nerve (*arrowhead*) crossing the rostral branch of the SCA (*dashed arrow*) along left tentorium cerebelli, and the right trochlear nerve entering the trochlear groove (*arrow*).

was visible in the ambient cistern 93% of the time. The nerve was always seen through its course in the trochlear groove, while it was confidently seen in 74% of cases piercing the posterior wall of the cavernous sinus surrounded by varying amounts of CSF in the so-called trochlear cistern. The T2 TSE sequence offered no effective contrast for visualization of the cavernous segment traveling within the fibrous layers of the lateral cavernous dura or the orbital segments, which were, therefore, not evaluated in this study.

The Table shows the visibility of the trochlear nerve segments from its origin to the cavernous sinus.

Trochlear Nerve Anatomy on 7T MRI Sections

Origin from the Brainstem. The origin of the trochlear nerve was seen at the posterior aspect of the pontomesencephalic junction at the inferior margin of inferior colliculus (Fig 1). In all subjects, the rostral branches of the superior cerebellar artery (SCA) were seen coursing above the nerve origin, whereas the caudal SCA branches traversed below it on the superior surface of the cerebellum (Fig 1).

Cisternal Segment. Anterior to its origin, the nerve was seen coursing superiorly and anterolaterally into the ambient cistern to reach the inferior surface of the free edge of the tentorium cerebelli (Fig 2). In 7% of the scans, CSF flow artifacts obscured the entire segment in the ambient cistern (Fig 2). The diameter of the trochlear nerve ranged between 0.4 and 0.5 mm in the ambient cistern.

On reaching the free edge of the tentorium cerebelli, the nerve traveled anterosuperiorly, becoming cranial to the rostral SCA branch before entering the trochlear groove (Fig 3).

Tentorial Segment. The trochlear nerve then passed through a 4- to 6-mm-long depression, ie, the trochlear groove, in the medial surface near the free edge of the tentorium before entering the cavernous sinus (Fig 4). The distance of the groove from the free edge was 1.1–2.0 mm (mean, 1.5 mm), and its depth measured between 0.4 and 0.9 mm (mean, 0.6 mm). After traversing the trochlear groove, the nerve pierced the posterior petroclinoid ligament to enter the lateral wall of the cavernous sinus, posterior and inferior to the oculomotor cistern (Fig 5). At this level, the nerve was always contained within its own CSF sleeve, the trochlear cistern, and was never seen in the oculomotor cistern (Fig 5). The caliber of the trochlear cistern, seen as a sleeve of CSF surrounding the trochlear nerve, varied considerably among the subjects.

Cavernous Segment. After piercing the posterior petroclinoid ligament, the nerve reached the posterolateral apex of the cavernous sinus within the trochlear cistern, wedged between the anterior petroclinoid ligament laterally and the posterior petroclinoid ligament medially (Fig 6). Thereafter, it continued anteriorly in the lateral wall of the cavernous sinus, immediately below the

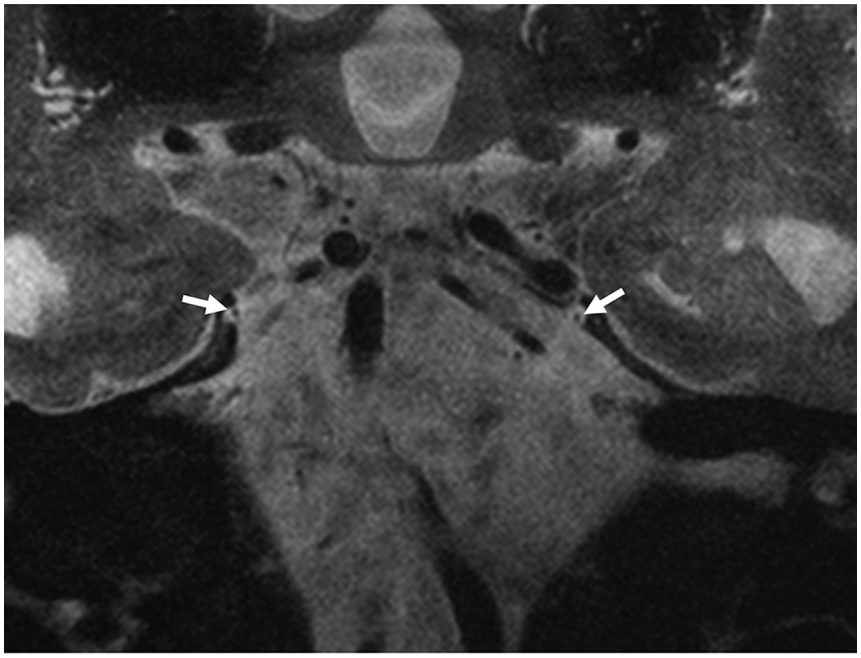

FIG 4. Coronal T2-weighted image showing the trochlear nerves within the trochlear grooves (*arrows*).

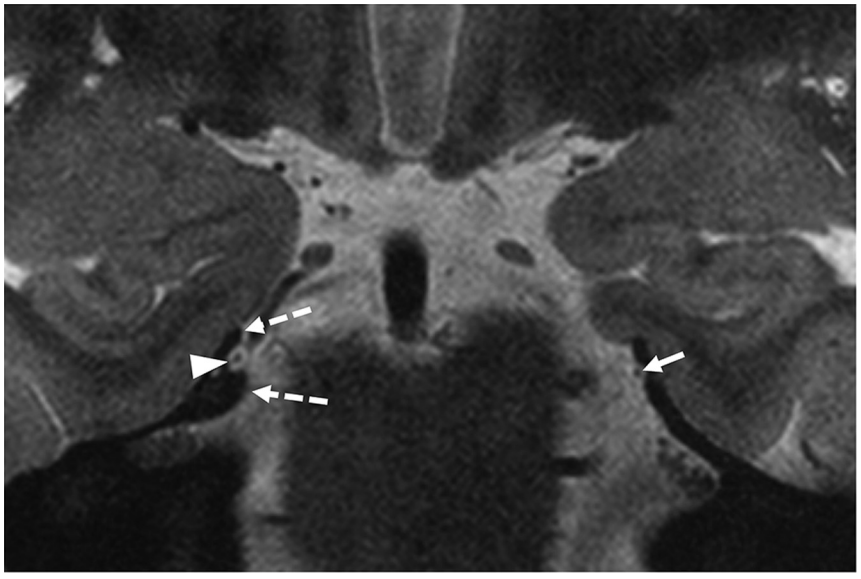

FIG 5. Coronal T2-weighted image showing the right trochlear nerve piercing the dura through the posterior petroclinoid ligament (*dashed arrows*) encased within the posterior end of the trochlear cistern (*arrowhead*), and the left trochlear nerve within the trochlear groove before entering the trochlear cistern (*arrow*).

oculomotor nerve and lateral to the cavernous venous channels and ICA (Fig 7).

Owing to the rather limited contrast between the nerve and adjacent structures on the TSE T2 sequence, the trochlear nerve could not be identified anterior to the midcavernous sinus in our study.

DISCUSSION

The aim of this study was to evaluate the ability of 7T MR imaging to better visualize the trochlear nerve and describe its course from its origin to the cavernous sinus in a large cohort of subjects with preserved nerve anatomy and normal ocular motor function. We were able to identify the trochlear nerve and its anatomic relationships with a high degree of consistency on our coronal high-resolution 2D T2 TSE sequence. 7T MR imaging is, therefore, a promising tool for the clinical imaging of the trochlear nerve.

Successful identification of the trochlear nerve on conventional MR imaging has remained challenging owing to its size, proximity to adjacent vessels/other structures, and the achievable spatial resolution of MR imaging at standard field strengths.[5,9] As also noted by Choi et al,[5] reducing the voxel size below the diameter of the trochlear nerve is critical in detecting the nerve. Previous MR imaging studies at 3T have shown limited success in consistently identifying the nerve throughout its course.[5,10-12] Consequently, there are incomplete and inconsistent descriptions of the trochlear nerve in the MR imaging literature, particularly in reference to the tentorial segment of the nerve and the trochlear cistern. Moreover, there is little-to-no reference in the imaging literature to the relationship of the nerve to the vessels in the ambient cistern and the dural reflections of the posterior cavernous sinus. Inconsistencies are also encountered in cadaveric, anatomic descriptions. A few postmortem dissections have described the tentorial course of the nerve within the oculomotor cistern, while others note a distinct CSF-containing trochlear cistern, independent of the oculomotor cistern.[7,13-15]

We were able to address these knowledge gaps and controversies regarding the normal anatomy of the trochlear nerve. No variations of the nerve course were observed apart from the relative distance of the nerve to other cisternal structures. Within the tentorial segment, the trochlear groove for the nerve was consistently visualized; whenever the cavernous segment was visualized, the nerve always coursed through the posterior cavernous sinus in its own CSF sleeve (ie, the trochlear cistern). These observations are important advancements in our understanding of trochlear nerve anatomy.

Proper identification of the trochlear nerve on MR imaging can be of value both from a presurgical perspective and in cases of suspected trochlear nerve palsy. Imaging has occasionally proved useful in identifying nerve impingement after trauma or nerve absence in some congenital cases of trochlear nerve

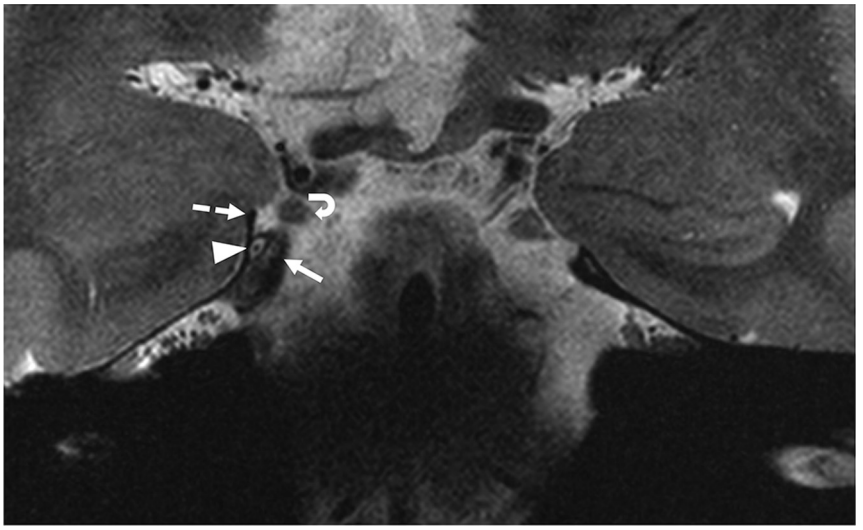

FIG 6. Coronal T2-weighted image showing the right trochlear nerve coursing in the trochlear cistern (*arrowhead*) at the posterolateral apex of cavernous sinus before reaching the lateral wall of the sinus and its relationships to the anterior petroclinoid (*dashed arrow*), the posterior petroclinoid (*arrow*) ligaments, and the right oculomotor nerve (*curved arrow*).

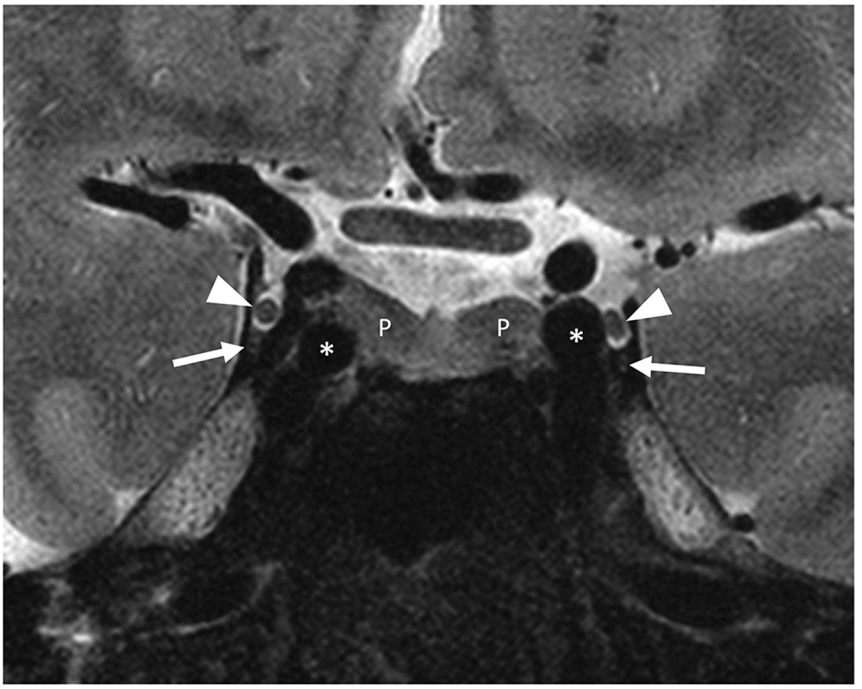

FIG 7. Coronal T2-weighted image showing the trochlear nerves within the lateral wall of middle one-third of the cavernous sinus (*arrows*), the oculomotor nerve and cistern (*arrowheads*), the pituitary gland (P), and the cavernous ICAs (*asterisks*).

palsy.[16-18] Currently, imaging is rarely used in the clinical evaluation of isolated trochlear nerve palsy, largely because of the inability of current techniques to achieve sufficient resolution to identify the nerve. Our observations show that high-resolution 2D TSE MR imaging at 7T permits reliable identification of the trochlear nerve and evaluation of its anatomic relationships.

The 3D techniques commonly used for cranial nerve assessment at lower field strengths, such as CISS, true FISP, and sampling perfection with application-optimized contrasts by using different flip angle evolution (SPACE sequence; Siemens), have limited data for cranial nerve assessment at 7T. These 3D techniques present unique challenges at ultra-high-field imaging. Due to the sensitivity of CISS and true FISP to phase variations, these techniques have artifacts at ultra-high-field strengths, limiting their use.[8] While volumetric TSE, such as T2 SPACE, can be advantageous at 7T due to higher SNR and reduced blurring at shorter echo-train lengths, minimal blurring can still limit visualization of small structures, such as CN IV. Additionally, pronounced inhomogeneity in the B_1+ transmit field at 7T limits use of variable flip angle sequences (eg, SPACE). Strategies to improve B_1+ homogeneity, such as parallel transmission, also add to the already high SAR of these sequences limiting achievable resolution in reasonable acquisition times. Given these limitations, we chose an optimized 2D TSE sequence to provide extremely high in-plane resolution to enable visualization of the small nerve while minimizing the section thickness to balance the SAR and scan length. Previous studies using TSE at 7T were unsuccessful in visualizing CN IV, which underscores the value and novelty of our sequence optimization.[8]

Our study has notable limitations. There were no children in our cohort; the application to children is limited by the current weight restrictions of 7T imaging to patients of >30 kg due to the SAR. Furthermore, our study did not include patients with suspected trochlear nerve pathology.

CONCLUSIONS

High-resolution 2D TSE MR imaging at 7T allows reliable visualization of the trochlear nerve in an acceptable acquisition time and appears promising for clinical imaging of the trochlear nerve.

Disclosure forms provided by the authors are available with the full text and PDF of this article at www.ajnr.org.

REFERENCES

1. Keane JR. **Fourth nerve palsy: historical review and study of 215 inpatients.** *Neurology* 1993;43:2439–43 CrossRef Medline

2. Brazis PW. **Isolated palsies of cranial nerves III, IV, and VI.** *Semin Neurol* 2009;29:14–28 CrossRef Medline
3. Altintas AG. **Trochlear nerve palsy: a review of etiology, incidence, diagnostic methods, and treatment alternatives.** *Arch Neurol Neurosci* 2020;7:1–5 CrossRef
4. Villain M, Segnarbieux F, Bonnel F, et al. **The trochlear nerve: anatomy by microdissection.** *Surg Radiol Anat* 1993;15:169–73 CrossRef Medline
5. Choi BS, Kim JH, Jung C, et al. **High-resolution 3D MR imaging of the trochlear nerve.** *AJNR Am J Neuroradiol* 2010;31:1076–79 CrossRef Medline
6. Ammirati M, Musumeci A, Bernardo A, et al. **The microsurgical anatomy of the cisternal segment of the trochlear nerve, as seen through different neurosurgical operative windows.** *Acta Neurochir (Wien)* 2002;144:1323–27 CrossRef Medline
7. Bunch PM, Kelly HR, Zander DA, et al. **Trochlear groove and trochlear cistern: useful anatomic landmarks for identifying the tentorial segment of cranial verve IV on MRI.** *AJNR Am J Neuroradiol* 2017;38:1026–30 CrossRef Medline
8. Grams AE, Kraff O, Kalkmann J, et al. **Magnetic resonance imaging of cranial nerves at 7 Tesla.** *Clin Neuroradiol* 2013;23:17–23 CrossRef Medline
9. Yousry I, Moriggl B, Dieterich M, et al. **MR anatomy of the proximal cisternal segment of the trochlear nerve: neurovascular relationships and landmarks.** *Radiology* 2002;223:31–38 CrossRef Medline
10. Yousry I, Camelio S, Schmid UD, et al. **Visualization of cranial nerves I-XII: value of 3D CISS and T2-weighted FSE sequences.** *Eur Radiol* 2000;10:1061–67 CrossRef Medline
11. Fischbach F, Müller M, Bruhn H. **High-resolution depiction of the cranial nerves in the posterior fossa (N III–N XII) with 2D fast spin echo and 3D gradient echo sequences at 3.0 T.** *Clin Imaging* 2009;33:169–74 CrossRef Medline
12. Cheng YS, Zhou ZR, Peng WJ, et al. **Three-dimensional-fast imaging employing steady-state acquisition and T2-weighted fast spin-echo magnetic resonance sequences on visualization of cranial nerves III - XII.** *Chin Med J (Engl)* 2008;121:276–79 Medline
13. Iaconetta G, de Notaris M, Benet A, et al. **The trochlear nerve: microanatomic and endoscopic study.** *Neurosurg Rev* 2013;36:227–38 CrossRef Medline
14. Lu D, Chen B, Liang Z, et al. **Comparison of bone marrow mesenchymal stem cells with bone marrow-derived mononuclear cells for treatment of diabetic critical limb ischemia and foot ulcer: a double-blind, randomized, controlled trial.** *Diabetes Res Clin Pract* 2011;92:26–36 CrossRef Medline
15. Everton KL, Rassner UA, Osborn AG, et al. **The oculomotor cistern: anatomy and high-resolution imaging.** *AJNR Am J Neuroradiol* 2008;29:1344–48 CrossRef Medline
16. Ko YS, Yang HJ, Son YJ, et al. **Delayed trochlear nerve palsy following traumatic subarachnoid hemorrhage: usefulness of high-resolution three dimensional magnetic resonance imaging and unusual course of the nerve.** *Korean J Neurotrauma* 2018;14:129–33 CrossRef Medline
17. Kim JH, Hwang JM. **Imaging of cranial nerves III, IV, VI in congenital cranial dysinnervation disorders.** *Korean J Ophthalmol* 2017;31:183–93 CrossRef Medline
18. Yang HK, Lee DS, Kim JH, et al. **Association of superior oblique muscle volumes with the presence or absence of the trochlear nerve on high-resolution MR imaging in congenital superior oblique palsy.** *AJNR Am J Neuroradiol* 2015;36:774–78 CrossRef Medline